

Giant Planar Hall Effect in the Dirac Semimetal ZrTe_5

P. Li[†], C.H. Zhang[†], J.W. Zhang, Y. Wen, and X.X. Zhang^{*}

King Abdullah University of Science and Technology (KAUST), Physical Science and Engineering Division (PSE), Thuwal 23955-6900, Saudi Arabia

* xixiang.zhang@kaust.edu.sa

Exploration and understanding of exotic topics in quantum physics such as Dirac/Weyl semimetals have become highly popular in the area of condensed matter. It has recently been predicted that a theoretical “giant planar Hall effect” can be induced by a chiral anomaly in Dirac/Weyl semimetals. ZrTe_5 is considered an intriguing Dirac semimetal at the boundary of weak and strong topological insulators, though this claim is still controversial. In this study, we report the observation in ZrTe_5 of giant planar Hall resistivity. We have also noted three different dependences of this resistivity on the magnetic field, as predicted by theory; maximum planar Hall resistivity occurs at the Lifshitz transition temperature. In addition, we have discovered a nontrivial Berry phase, as well as a chiral-anomaly-induced negative longitudinal and a giant in-plane anisotropic magnetoresistance. All these experimental observations coherently demonstrate that ZrTe_5 is a Dirac semimetal.

As new quantum material types, Dirac/Weyl semimetals have drawn tremendous recent attention for their potential applications in physics.[1-8] A number of exotic and intriguing transport properties have been observed in these topological materials, which are closely associated with the existence of quasiparticles (Weyl electrons): e.g., massless and defined fermion chirality. One of the most intriguing magnetotransport properties is the chiral-anomaly-induced negative magnetoresistance (NMR) in nonmagnetic Dirac or Weyl semimetals with broken inversion symmetry.[5,9,10] Although NMR is considered a signature of such materials, several extrinsic factors – such as current jetting and conductance fluctuation – may also cause the same effect.[11-14] Recently, the giant planar Hall effect (PHE), an intriguing transport phenomenon, has been predicted to appear in Dirac/Weyl semimetals;[15,16] the PHE refers to the transverse voltage when a magnetic field is applied in-plane to the electrical current. It is a weak magnetic field effect typically observed in ferromagnetic materials, and it originates from spin-orbit coupling.[17-19] Unlike in the case of ferromagnetic materials, the PHE in topological Dirac/Weyl semimetals has been theoretically demonstrated to derive from the nontrivial Berry phase and chiral anomaly;[15,16] along with NMR, it is characteristic of topological Dirac/Weyl semimetals.[20-24] The angular dependence of PHE resistivity and longitudinal anisotropic magnetoresistance (AMR) in Dirac/Weyl semimetals can be described as[15,16]

$$\rho_{xy} = -\Delta\rho_{xy}^{\text{chiral}} \sin\varphi \cos\varphi \quad (1)$$

$$\rho_{xx} = \rho_{\perp} - \Delta\rho_{xy}^{\text{chiral}} \cos^2\varphi \quad (2)$$

where $\Delta\rho_{\text{chiral}} = \rho_{\perp} - \rho_{\parallel}$ is the resistivity anisotropy induced by the chiral anomaly and Berry phase, and ρ_{\perp} and ρ_{\parallel} are the resistivities for magnetic fields applied transversely and in parallel, respectively, to the current in the plane.

The ZrTe₅ monolayer was initially predicted to be a 2D quantum spin Hall insulator; this was later confirmed by scanning tunneling spectroscopy.[25-27] Although angle-resolved photoemission spectroscopy (ARPES) experiments directly demonstrated that a bulk ZrTe₅ is a weak topological insulator (TI),[28] it was revealed to be a 3D Dirac semimetal through the observation of chiral anomaly in magnetotransport[29] and a nontrivial Berry phase,[30,31] and by magneto-infrared spectroscopy.[32] More interestingly, Dirac semimetal states have been known to appear in ZrTe₅ at the boundary of strong and weak TIs.[33,34] The hydrostatic pressure experiment has suggested that the nontrivial Berry phase in the quasi-3D Dirac semimetal ZrTe₅ would fade with increasing pressure[35]. The exact nature of the layered transition metal chalcogenide ZrTe₅, therefore, remains hotly debated, and more evidence is needed to uncover its Dirac semimetal state.

In this letter, we report the observation of the chiral-anomaly-induced PHE in ZrTe₅ nanoplates. The nontrivial Berry phase ($\sim\pi$) was obtained from the Shubnikov de Haas (SdH) oscillation data. The chiral-anomaly-induced giant planar Hall resistivity reached a maximum of 254 $\mu\Omega$ cm (14 T) near the resistivity anomaly temperature \sim 150 K, which strongly supports the existence of a Dirac point in ZrTe₅.

High-quality single ZrTe₅ crystals grown by iodine-assisted vapor transport were obtained from the company HQ Graphene. Owing to the relatively weak van der Waals force along the *b*-axis, the thin ZrTe₅ plates were mechanically exfoliated onto the SiO₂(280 nm)/Si substrates from bulk single crystals. The Ti(10 nm)/Au(70 nm) electrodes were patterned via standard e-beam lithography and deposited by e-beam evaporation. The magneto-transport measurements were carried out on a physical property measurement system (Dynacool system, Quantum Design Inc.) using standard lock-in and four-probe methods.[36] Imaging of the ZrTe₅ crystal structure was performed using monochromated Cs-corrected high-resolution scanning transmission electron microscopy (STEM, Titan 80-300, FEI).

Figure 1(a) presents the optical image of a typical exfoliated ZrTe₅ micro-ribbon device and the measurement configurations of PHE (ρ_{xy}) and AMR (ρ_{xx}).^[36] The high-angle area dark-field (HAADF) image of ZrTe₅ (*ab*-plane) in Fig. 1(b) suggests optimal sample crystallinity. The ZrTe₅ unit cell in the *ab*-plane is indicated by the white dashed rectangle, in which Zr and Te atoms are highlighted with green and purple dots for clarity. From this HAADF image, the lattice constant along *b* is identified to be ~ 14.5 Å. According to the previous report,^[33,34] ZrTe₅ will transform from strong to weak TIs by increasing the lattice constant *b* to a value greater than 14.46 Å, whereas the Dirac semimetal states will appear at the transformation boundary. The lattice constant of our sample therefore supports the prediction of the Dirac semimetal state in ZrTe₅.

Figure 1(c) illustrates the typical temperature dependence of the longitudinal resistance of ZrTe₅ under magnetic fields of 0 and 14 T. The current is along the *a*-axis of ZrTe₅ in Fig 1(a). In accordance with previous results, a pronounced resistance anomaly, the metal-insulator transition (MIT), appeared at ~ 135 K in the zero-field curve.^[37,38] The transition temperature notably rose to ~ 150 K as the magnetic field increased to 14 T. This MIT transition can be ascribed to the Lifshitz transition^[39], accompanied by a change of the dominated carrier from *p*-type (high temperatures) to *n*-type (low temperatures).^[28] Not surprisingly, we also observed such a transition in Hall resistance near 135 K, as noted in Fig 1(d) and its inset.^[36] The nonlinear Hall resistance in ZrTe₅ under low magnetic fields in Fig. 1(d) has been frequently observed in previous reports,^[40,41] which are interpreted within the two-band model framework.^[38,39]

To explore the physics of the quantum magneto-transport underlying the experimental data (see Fig. 2(a)), we calculated dR/dH from the transverse magnetoresistance measured with the magnetic field applied perpendicular to the current ($H//b$ -axis) and in the current plane to reveal

the SdH oscillations. The oscillations are evident in the dR/dH curves as a function of H^1 for different temperatures (Fig. 2(b)). A small shoulder at $H = 5.3$ T, indicated by the arrow, can be attributed to spin splitting.[30] To extract the Berry phase, we plotted the Landau fan diagram in Fig. 2(c). According to the Lifshitz-Onsager quantization rule, $B_F / H = n - \gamma + \delta$, where n , B_F , and γ are the Landau index, oscillation frequency, and Onsager phase factor ($\gamma = 1/2 - \phi_B / 2\pi$), respectively. The variable δ is an additional phase shift within $\pm 1/8$ that depends on the degree of the Fermi surface dimensionality. The Berry phase ϕ_B can then be obtained from the intercept of the Landau fan curve in Fig. 2(c). To avoid high-field spin splitting effects on the Berry phase determination,[6] we only linearly fitted the Landau index with $n > 3$ as a function of H^1 . From the intercept value of -0.036, we found a nontrivial Berry phase $\phi_B = 1.072\pi$.[36]

This nontrivial Berry phase motivated us to further explore the chiral-anomaly-induced NMR and other exotic transport properties. Figure 2(d) highlights the longitudinal MR at different temperatures. In addition to the pronounced SdH oscillations, negative MR was clearly noted at low temperatures ($T < 40$ K) under strong magnetic fields. Based on the geometry of our devices, we can exclude the contribution of current jetting to the observed NMR.[11,12,36]

The nontrivial Berry phase and NMR support the existence of a topological semimetal state in ZrTe_5 and suggest that a giant PHE could be observed in the material.[15,16,20-23] We then measured the PHE and AMR on the same devices. Figures 3(a) to (c) illustrate the angular dependence of the planar Hall resistance R_{xy}^{planar} of ZrTe_5 at different temperatures, where the sample is rotating in the ac -plane under magnetic fields of +14 and -14 T, respectively. The apparent R_{xy}^{planar} measured at 2 and 200 K and under both fields do not exhibit thorough $\sin 2\varphi$ (φ : angle between H and I in the ac -plane) dependence (Eq. (1)) , but the data measured at 150 K

does. Another interesting feature is that the main peak in $R_{xy}^{\text{planar}} \sim \varphi$ curves for $H = 14$ T shifts gradually from $\sim 310^\circ$ below 150 K to $\sim 130^\circ$ above 150 K. Based on Fig. 1d, we can surmise that the dominated carrier type changes from n to p at around 135 K. This asymmetric angular dependence of R_{xy}^{planar} may be due to a normal Hall effect arising from the perpendicular component of the applied magnetic field. This perpendicular component could be easily caused by sample surface (ac -plane) misalignment with respect to the magnetic field. Figure 3(d) presents a schematic configuration of the misalignment. The yellow ring indicates the ideal magnetic field rotation, whereas the actual situation is represented by the blue circle. Owing to the rather small carrier density in ZrTe_5 (on the scale of 10^{17} cm^{-3}), [30] even a tiny perpendicular magnetic component can lead to significant normal Hall resistance that affects the measured data.

To distinguish the normal Hall contribution from R_{xy}^{planar} , we calculated the average measured $R_{xy}^{\text{planar}} \sim \varphi$ under -14 and 14 T. We expect to remove the normal Hall contribution by summing the measured data under both positive and negative fields, as illustrated by the green curves in Figs. 3(a) to- 3(c). We found that R_{xy}^{planar} typically becomes much more symmetric (Fig. 3(e)) and displays a two-fold feature over 360° . The data, however, cannot be described directly by Eq. (1) due to a resistance shift of 7.5Ω away from zero. This shift could be attributed to longitudinal resistance misalignment during the fabrication of Hall bar device. This small contribution can be accounted for by fitting the averaged data to Eq. (3):

$$R_{xy}^{\text{planar}} = -\Delta\rho_{xy}^{\text{chiral}} \sin \varphi \cos \varphi + a\Delta\rho_{xy}^{\text{chiral}} \cos^2 \varphi + b \quad (3)$$

The first term in the above equation is the intrinsic PHE originating from the chiral anomaly; the second and third terms are, respectively, the in-plane AMR and longitudinal resistance offset

caused by misalignment of the Hall bar. Compared to the standard longitudinal AMR observed in these devices (Figs. 4(a)), however, the angular-dependent longitudinal misalignment resistance is quite small, which is evident from the minor resistance shift in Hall effect (Fig. 1(d)). Hence, the value of a in Eq.(3) should be quite small. After taking the longitudinal Hall bar misalignment resistance b into account, R_{xy}^{planar} can be well fitted using Eq. (3), as demonstrated by the red line in Fig. 3(e). To exclude any artifacts in the raw data analysis, we also fitted the measured R_{xy}^{planar} directly with three contributions: the two-fold PHE, one-fold Hall effect, and resistance offset due to misalignment of the Hall bar. Figure 3(f) yields the measured angular-dependent R_{xy}^{planar} (200 K, 14 T) and three fitting curves. We found that the amplitude of the intrinsic R_{xy}^{planar} obtained from the above two fitting strategies are identical – namely, -3.35Ω in Fig. 3(e) and -3.33Ω in Fig. 3(f) – which suggests that both methods produce nearly the same intrinsic R_{xy}^{planar} .

As a comparison, we measured the longitudinal AMR ($\text{AMR} = (R_{\phi} - R_{\perp}) / R_{\perp}$) at different temperatures, as highlighted in Fig. 4(a). The exact 45° phase difference between the angular-dependent two-fold AMR and intrinsic PHE (Fig. 4(b)) agree with theoretical predictions and Eqs. (1) and (2).[15,16,36] Generally, the AMR in conventional magnetic materials is quite small and caused by spin-orbit coupling.[17] The large AMR in this study reached a maximum of -43% at 2 K and 14 T, which is believed to be closely related to the giant PHE induced by the chiral anomaly.[21,22] Figure 4(b) presents the angular-dependent intrinsic planar Hall resistivity $\rho_{xy}^{\text{chiral}}$ at several selected magnetic fields. The value of $\rho_{xy}^{\text{chiral}}$ grows monotonically to $254 \mu\Omega \text{ cm}$ as the magnetic field is increased to 14 T. The PHE observed in our ZrTe_5 device is about four orders of magnitude higher than that noted in conventional ferromagnetic metals.[19]

To gain deeper insight into the physical mechanism underlying this giant PHE, we extracted the field dependence of the amplitude of the intrinsic planar Hall resistivity $\rho_{xy}^{\text{chiral}}$ at 150 K and plotted it in Fig 4(c).[36] The variable $\rho_{xy}^{\text{chiral}}$ does not appear to exhibit any simple linear or quadratic relation to the magnetic field H , unlike the field-dependent MR and Hall observed in conventional ferromagnetic materials.[17,18] Instead, it displays roughly three different field-dependences, based on the strength of magnetic field: for low fields ($H < 3$ T), $\rho_{xy}^{\text{chiral}}$ depends on H^2 ; in the range of $5 \text{ T} < H < 9 \text{ T}$, $\rho_{xy}^{\text{chiral}}$ varies linearly with H ; and at $H > 9 \text{ T}$, $\rho_{xy}^{\text{chiral}}$ demonstrates a weak tendency toward saturation as a function of H . It has been theoretically predicted that the chiral-anomaly-induced PHE can be divided into three field regions:[15]

$$L_a \gg L_c, \quad \rho_{xy}^{\text{chiral}} \propto \left(\frac{L_c}{L_a}\right)^2 \propto H^2; \text{ weak} \quad (4)$$

$$L_a < L_x < \frac{L_c^2}{L_a}, \quad \rho_{xy}^{\text{chiral}} \propto \frac{L_a}{L_x} \propto H; \text{ intermediate} \quad (5)$$

$$L_a \ll L_c, \quad \rho_{xy}^{\text{chiral}} \propto \frac{L_a^2}{L_c^2} \left(1 + \frac{2L_c^2}{L_a L_x}\right) \propto \frac{1}{H^2}(1 + H); \text{ strong} \quad (6)$$

where L_x , L_a , and L_c are the sample, magnetic ($L_a \propto H^{-1}$), and chiral charge diffusion lengths, respectively.[15] The intrinsic chiral-anomaly-induced planar Hall resistivity $\rho_{xy}^{\text{chiral}}$ should obviously exhibit three different magnetic field dependences if the applied field is large enough. The consistency between our observation and theory is strong evidence of a topological state in our sample.

To understand the behavior of $\rho_{xy}^{\text{chiral}}$ in more detail, we charted, in Fig. 4(d), the temperature-dependent amplitude of the planar Hall resistivity measured at 14 T, which is

extracted from the inset (angular dependence of $\rho_{xy}^{\text{chiral}}$ at different temperatures). Interestingly, a strong peak in the curve of the temperature-dependent intrinsic $\rho_{xy}^{\text{chiral}}$ appears at ~ 150 K, near the MIT temperature. This peak behavior of $\rho_{xy}^{\text{chiral}}(T)$ is different from the monotonic decrease of $\rho_{xy}^{\text{chiral}}$ with increasing temperature observed in some Dirac/Weyl semimetals.[20-23] An ARPES study revealed that[28] the Fermi level in ZrTe_5 sweeps from an electron-like band to a hole-like one across the MIT temperature, though no definite evidence can be found to support the existence of a Dirac cone in the ARPES spectra.[28] Our observation of a giant PHE and its interesting behavior in Fig. 4(d) provides strong support for the existence of Dirac fermions in ZrTe_5 , since the giant PHE is caused by the chiral anomaly and Berry phase of carriers near the Dirac point.[15,16] When the Fermi level in ZrTe_5 sweeps across the Dirac crossing point, the chiral-anomaly-induced intrinsic $\rho_{xy}^{\text{chiral}}$ is enhanced near the MIT temperature (Fig. 4(d)). Nevertheless, in other well-known Dirac/Weyl semimetals such as Cd_3As_2 , GdPtBi , and WTe_2 , [20-23] the Dirac point deviates much more from the Fermi level as the temperature increases.[42,43] A monotonic decrease in $\rho_{xy}^{\text{chiral}}$ with increasing temperature is therefore observed in these Dirac/Weyl semimetals.

To conclude, we have observed a giant PHE and a nontrivial Berry phase, along with negative longitudinal and large AMR, in ZrTe_5 ; this fully demonstrates that ZrTe_5 is indeed a Dirac semimetal.

Peng Li and Chenhui Zhang have contributed equally to this work. We thank Professor Feng Liu at the University of Utah for his helpful discussions. The research presented in this publication was supported by funding from the King Abdullah University of Science and

Technology (KAUST). Li acknowledges the financial support of CRF-2015-SENSORS-2709 (KAUST).

References

- [1] Z. Liu *et al.*, *Science* **343**, 864 (2014).
- [2] S. Parameswaran, T. Grover, D. Abanin, D. Pesin, and A. Vishwanath, *Phys. Rev. X* **4**, 031035 (2014).
- [3] B. Lv *et al.*, *Phys. Rev. X* **5**, 031013 (2015).
- [4] A. A. Soluyanov, D. Gresch, Z. Wang, Q. Wu, M. Troyer, X. Dai, and B. A. Bernevig, *Nature* **527**, 495 (2015).
- [5] J. Xiong, S. K. Kushwaha, T. Liang, J. W. Krizan, M. Hirschberger, W. Wang, R. Cava, and N. Ong, *Science* **350**, 413 (2015).
- [6] P. J. Moll, N. L. Nair, T. Helm, A. C. Potter, I. Kimchi, A. Vishwanath, and J. G. Analytis, *Nature* **535**, 266 (2016).
- [7] A. C. Potter, I. Kimchi, and A. Vishwanath, *Nat. Commun.* **5**, 5161 (2014).
- [8] P. Li *et al.*, *Nat. Commun.* **8**, 2150 (2017).
- [9] H. B. Nielsen and M. Ninomiya, *Phys. Lett. B* **130**, 389 (1983).
- [10] X. Huang *et al.*, *Phys. Rev. X* **5**, 031023 (2015).
- [11] R. Dos Reis, M. Ajeesh, N. Kumar, F. Arnold, C. Shekhar, M. Naumann, M. Schmidt, M. Nicklas, and E. Hassinger, *New J. Phys.* **18**, 085006 (2016).
- [12] F. Arnold *et al.*, *Nat. Commun.* **7**, 11615 (2016).
- [13] P. Goswami, J. Pixley, and S. D. Sarma, *Phys Rev B* **92**, 075205 (2015).
- [14] T. Schumann, M. Goyal, D. A. Kealhofer, and S. Stemmer, *Phys. Rev. B* **95**, 241113 (2017).
- [15] A. Burkov, *Phys. Rev. B* **96**, 041110 (2017).
- [16] S. Nandy, G. Sharma, A. Taraphder, and S. Tewari, *Phys. Rev. Lett.* **119**, 176804 (2017).
- [17] T. McGuire and R. Potter, *IEEE Tran. Magn.* **11**, 1018 (1975).
- [18] H. Tang, R. Kawakami, D. Awschalom, and M. Roukes, *Phys. Rev. Lett.* **90**, 107201 (2003).
- [19] S. Kokado, M. Tsunoda, K. Harigaya, and A. Sakuma, *J. Phys. Soc. Jpn.* **81**, 024705 (2012).
- [20] N. Kumar, C. Felser, and C. Shekhar, *arXiv preprint arXiv:1711.04133* (2017).
- [21] H. Li, H. Wang, H. He, J. Wang, and S.-Q. Shen, *arXiv preprint arXiv:1711.03671* (2017).
- [22] M. Wu *et al.*, *arXiv preprint arXiv:1710.01855* (2017).
- [23] Y. Wang, J. Gong, D. Liang, M. Ge, J. Wang, W. Zhu, and C. Zhang, *arXiv preprint arXiv:1801.05929* (2018).
- [24] S. Liang, J. Lin, S. Kushwaha, R. Cava, and N. Ong, *arXiv preprint arXiv:1802.01544* (2018).
- [25] H. Weng, X. Dai, and Z. Fang, *Phys. Rev. X* **4**, 011002 (2014).
- [26] X.-B. Li *et al.*, *Phys. Rev. Lett.* **116**, 176803 (2016).
- [27] R. Wu *et al.*, *Phys. Rev. X* **6**, 021017 (2016).
- [28] Y. Zhang *et al.*, *Nat. Commun.* **8**, 15512 (2017).
- [29] Q. Li *et al.*, *Nat. Phys.* **12**, 550 (2016).
- [30] Y. Liu *et al.*, *Nat. Commun.* **7**, 12516 (2016).
- [31] X. Yuan *et al.*, *NPG Asia Materials* **8**, e325 (2016).
- [32] R. Chen, Z. Chen, X.-Y. Song, J. Schneeloch, G. Gu, F. Wang, and N. Wang, *Phys. Rev. Lett.* **115**, 176404 (2015).
- [33] G. Manzoni *et al.*, *Phys. Rev. Lett.* **117**, 237601 (2016).
- [34] Z. Fan, Q.-F. Liang, Y. Chen, S.-H. Yao, and J. Zhou, *Sci. Rep.* **7**, 45667 (2017).
- [35] J. Zhang *et al.*, *Phys. Rev. Lett.* **118**, 206601 (2017).
- [36] See Supplemental Material at <http://link.aps.org/supplemental/> for Measurement configuration, Raman spectra, thickness determination by AFM, quantum oscillation for Berry phase, exclusion of current jetting, magnetic field dependence of planar Hall resistivity at different temperatures, temperature dependence of resistance anisotropy, and more AMR and PHE data.

- [37] G. Zheng *et al.*, Phys. Rev. B **93**, 115414 (2016).
- [38] J. Niu *et al.*, Phys. Rev. B **95**, 035420 (2017).
- [39] H. Chi, C. Zhang, G. Gu, D. E. Kharzeev, X. Dai, and Q. Li, New J. Phys. **19**, 015005 (2017).
- [40] T. Liang, Q. Gibson, M. Liu, W. Wang, R. Cava, and N. Ong, arXiv preprint arXiv:1612.06972 (2016).
- [41] H. Wang *et al.*, Phys. Rev. B **93**, 165127 (2016).
- [42] S. Borisenko, Q. Gibson, D. Evtushinsky, V. Zabolotnyy, B. Büchner, and R. J. Cava, Phys. Rev. Lett. **113**, 027603 (2014).
- [43] C. Wang *et al.*, Phys. Rev. B **94**, 241119 (2016).

Figure Captions

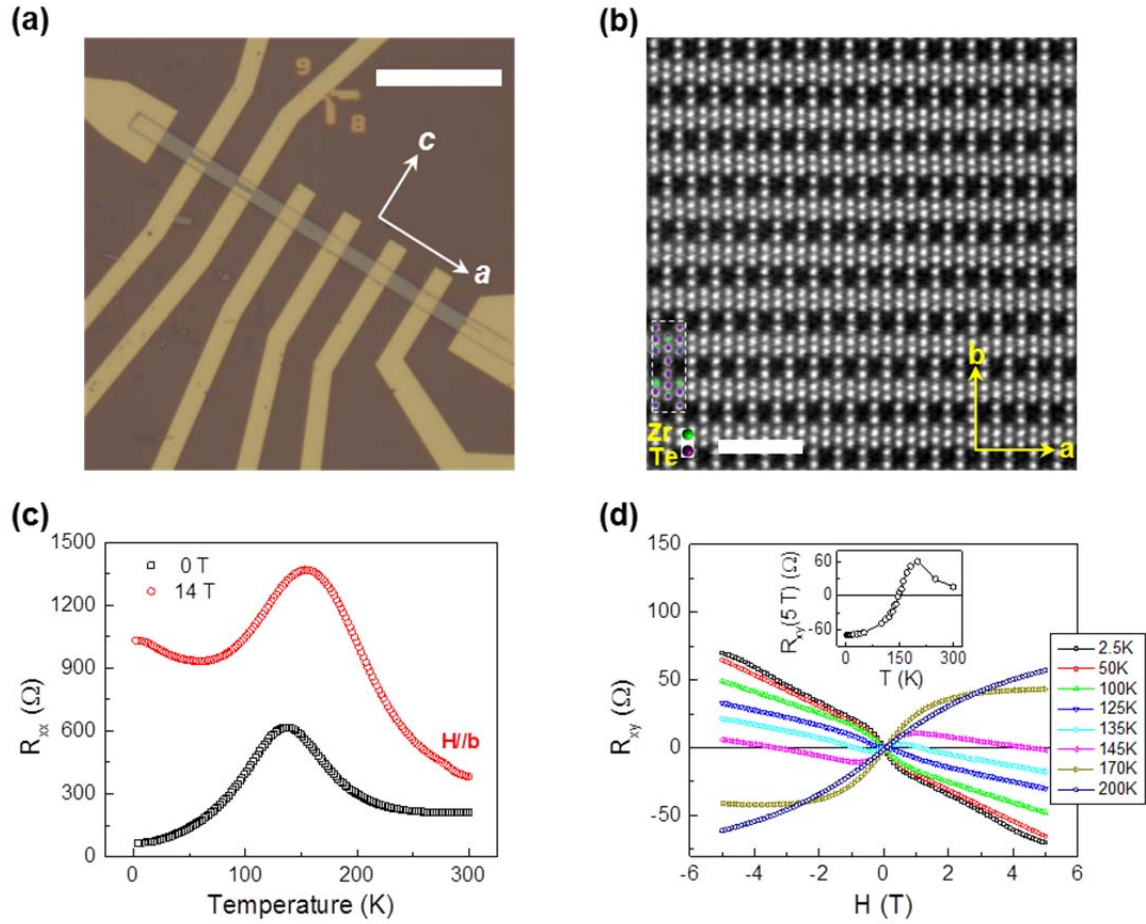


FIG. 1. (a) Optical image of ZrTe₅ devices. The white scale bar represents 30 μm. (b) An HAADF image of the ZrTe₅ sample in the *ab*-plane. The dashed rectangle represents the ZrTe₅ unit cell in the *ab*-plane. The green and purple dots are the Zr and Te atoms, respectively. The white scale bar is 1 nm. (c) Temperature dependence of ZrTe₅ resistance under different magnetic fields. (d) Hall resistance of ZrTe₅ as a function of magnetic field at selected temperatures. To indicate the transition of the dominated carrier type, the inset provides the temperature dependence of measured Hall resistance at 5 T.

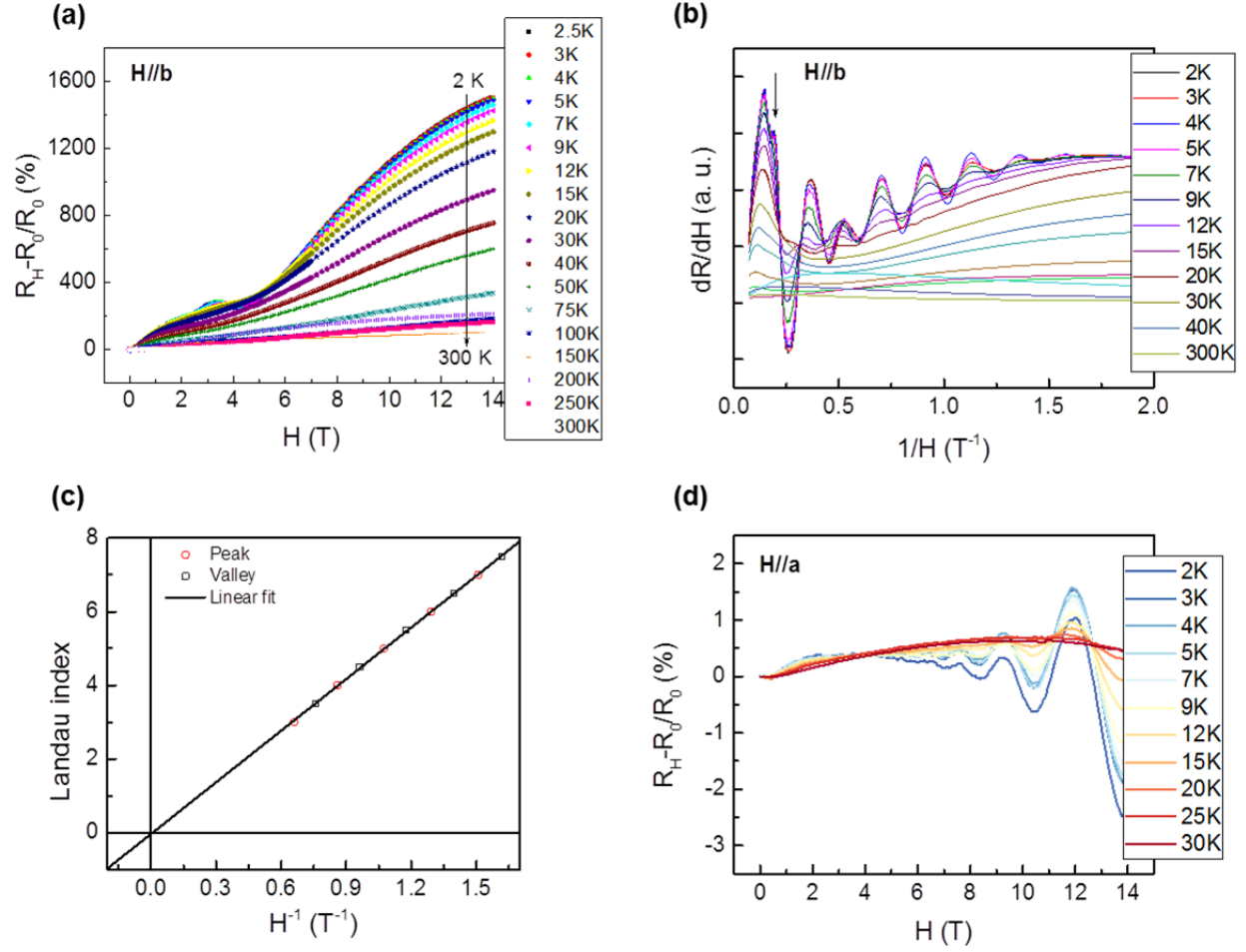


FIG. 2. (a) Magnetic field-dependent magnetoresistance ratio of ZrTe₅ with $H//b$. (b) Shubnikov de Haas oscillation amplitude as a function of inverse magnetic field at various temperatures. The arrow indicates spin splitting at high fields. (c) Landau fan diagram with an intercept of -0.036. We used the data with $n > 3$ to eliminate the influence of spin splitting on the Berry phase. (d) Longitudinal magnetoresistance with $H//a$ at different temperatures. Besides the strong SdH oscillations, the chiral-anomaly-induced NMR is distinguishable.

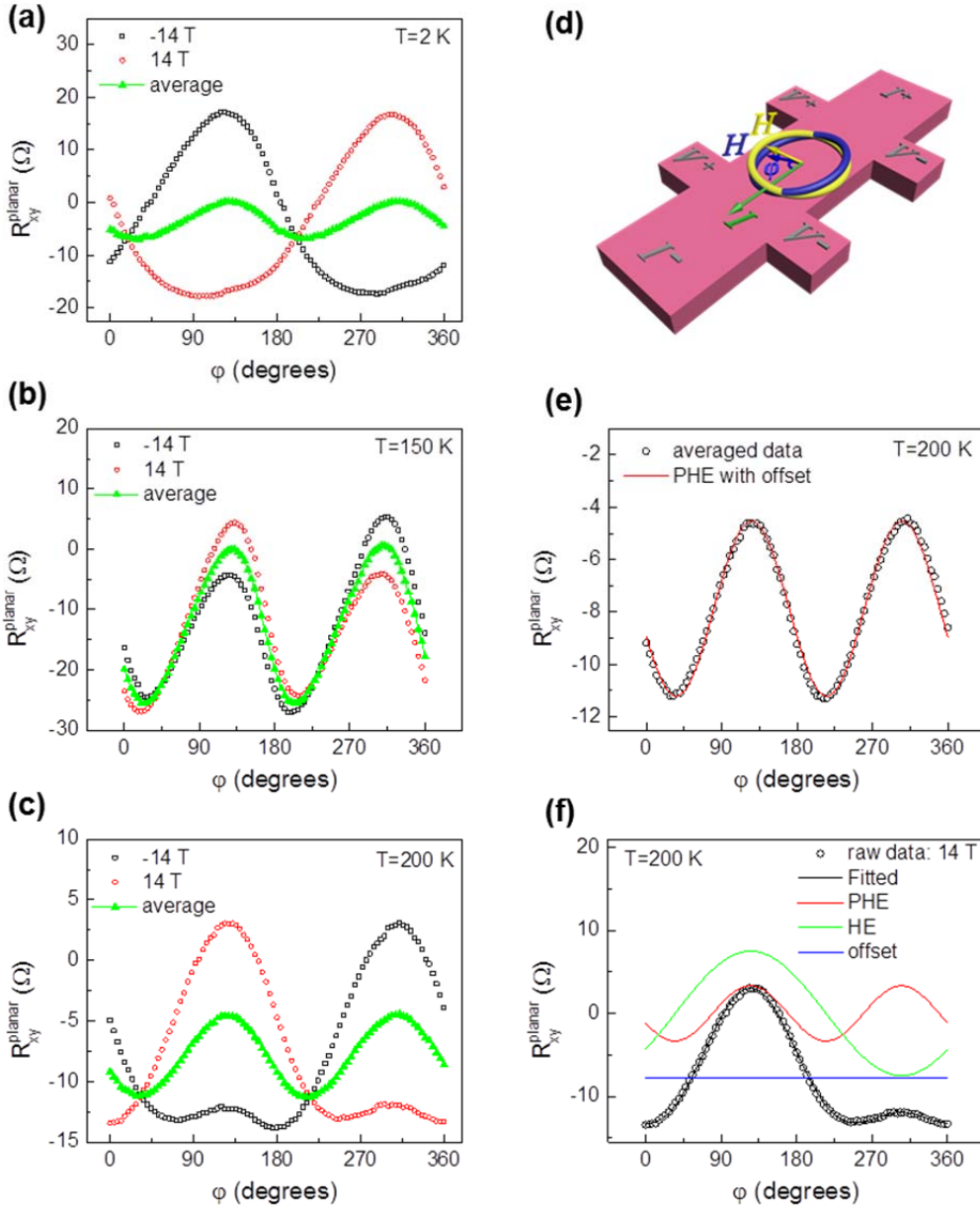


FIG. 3. Measured planar Hall resistance R_{xy}^{planar} of ZrTe_5 under opposite magnetic fields (14 and -14 T). (a) $T = 2$ K. (b) $T = 150$ K. (c) $T = 200$ K. (d) Schematic of the measurement configuration with misalignment that includes an out-of-plane magnetic field component. The yellow circle illustrates the ideal magnetic field rotation during the PHE measurement; the blue circle represents the real rotation with misalignment, which yields the Hall effect in the measured R_{xy}^{planar} . The phase shift of 180° between 2 and 200 K further indicates the contribution of magnetic field misalignment in the device plane. (e) Typical fitting of averaged R_{xy}^{planar} and fitting curves ($T = 200$ K). (f) Typical

fitting of angular-dependent R_{xy}^{planar} with three contributions: the intrinsic PHE, Hall effect, and longitudinal resistance offset. The longitudinal resistance comes from misalignment of the Hall bar, and its offset arises from such a misalignment during device fabrication.

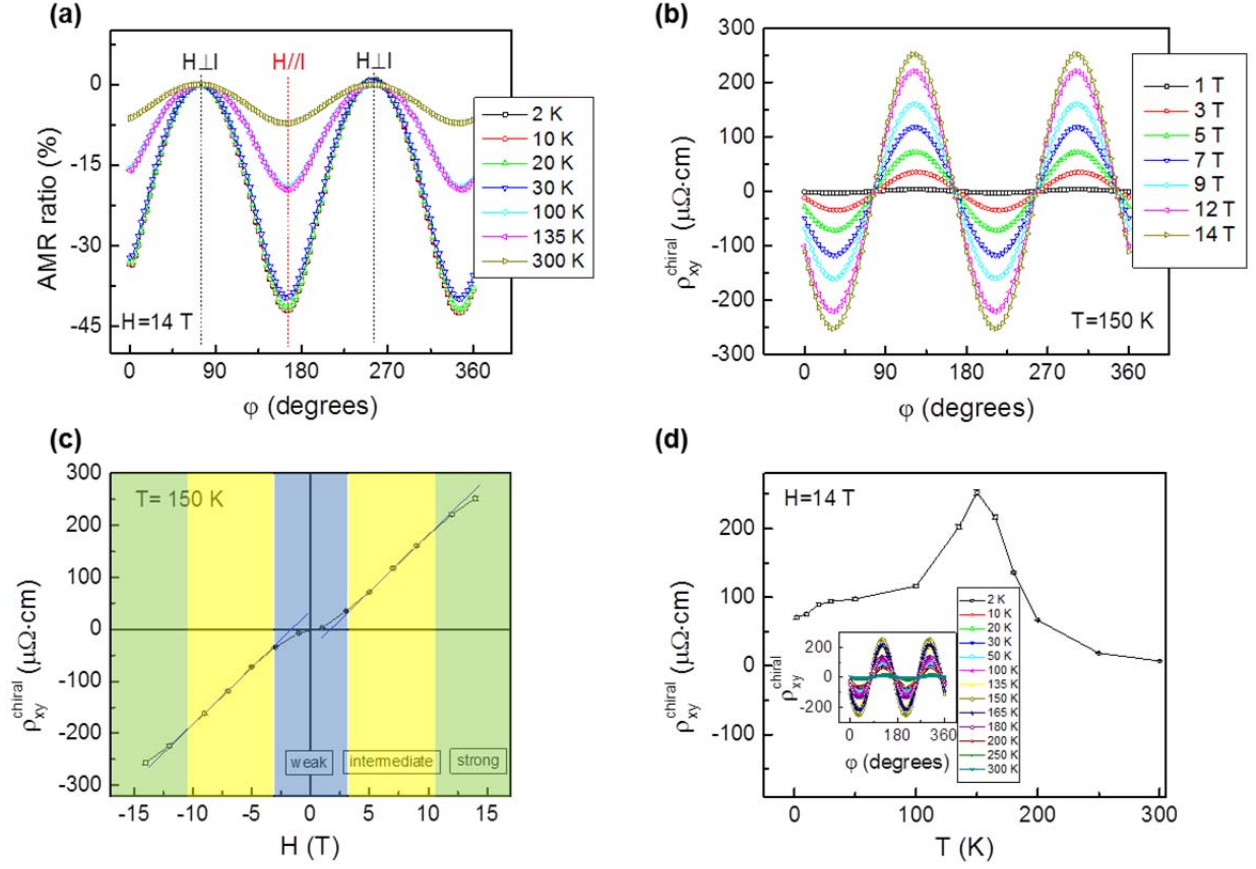


FIG. 4. (a) Measured in-plane anisotropic magnetoresistance of ZrTe₅ at various temperatures ($H = 14$ T). (b) Intrinsic planar Hall resistivity $\rho_{xy}^{\text{chiral}}$ as a function of rotation angle at different magnetic fields ($T = 150$ K). (c) Magnetic field dependence of chiral-anomaly-induced planar Hall resistivity $\rho_{xy}^{\text{chiral}}$. This can be divided into three regions. The line which represents linear dependence in the intermediate magnetic field region is a visual guide. The error bar is derived from the fitting via Eq. (3). (d) Intrinsic planar Hall resistivity $\rho_{xy}^{\text{chiral}}$ as a function of temperature ($H = 14$ T). The inset provides the corresponding angular-dependent $\rho_{xy}^{\text{chiral}}$ ($H = 14$ T).